HHS Public Access

Author manuscript

Nat Neurosci. Author manuscript; available in PMC 2016 October 25.

Published in final edited form as:

Nat Neurosci. 2016 June ; 19(6): 826–834. doi:10.1038/nn.4293.

Serotonin modulates spike probability in the axon initial segment through HCN channels

Kwang Woo Ko[1,2], **Matthew N. Rasband**[3], **Victor Meseguer**[4], **Richard H. Kramer**[4], and **Nace L. Golding**[1,2,‡]

[1] Department of Neuroscience, University of Texas at Austin, Austin, TX 78712

[2] Center for Learning and Memory, University of Texas at Austin, Austin, TX 78712

[3] Department of Neuroscience, Baylor College of Medicine, Houston, Texas 77030.

[4] Department of Molecular and Cell Biology, University of California, Berkeley, CA 94720, USA.

Abstract

The axon initial segment (AIS) serves as the site of action potential initiation in most neurons, but difficulties in isolating the effects of voltage-gated ion channels in the AIS from those of the soma and dendrites have hampered understanding how AIS properties influence neural coding. Here we have combined confocal microscopy, patch-clamp recordings and light-sensitive channel blockers ("photoswitches") in binaural auditory neurons to show that hyperpolarization and cyclic nucleotide-gated (HCN) channels are expressed in the AIS and decrease spike probability, distinct from the role of HCN channels in the soma and dendrites. Furthermore, the control of spike threshold by HCN channels in the AIS can be altered through serotonin modulation of 5-HT_{1A} receptors, which hyperpolarizes the activation range of HCN channels. As release of serotonin signals changes in motivation and attention states, axonal HCN channels provide a mechanism to translate these signals into changes in the threshold for sensory stimuli.

Introduction

In most neurons in the brain, excitatory and inhibitory postsynaptic potentials (EPSPs and IPSPs) interact with different types of voltage-gated channels in the dendrites, and the product of these interactions triggers patterns of action potential output in the axon. From classical studies it was hypothesized on the basis of indirect evidence that the site for action

‡To whom correspondence should be addressed Nace Golding, Department of Neuroscience, 1 University Station, C7000, University of Texas at Austin, Austin, TX 78712, golding@austin.utexas.edu.

Author Contributions Statement

K.W.K performed and analyzed all experiments in brain slices. M.N.R. performed and analyzed immunofluorescence labeling experiments. V.M. performed and analyzed experiments in HEK cells. R.H.K. and N.L.G. supervised and helped design experiments in expression systems and slices, respectively. K.W.K. and N.L.G. wrote the main manuscript text with assistance from M.N.R. and R.H.K. M.N.R. prepared **Fig. 1**, K.W.K. prepared **Figs. 2-8** and **Supplementary Figs. 2-7**, while V.M. and R.H.K. prepared **Supplementary Fig. 1**. All authors reviewed the manuscript.

A Supplementary Methods Checklist is available.

The authors declare no competing financial interests.

potential generation is the axon initial segment [1], later supported with simultaneous somatic and axonal recordings [2]. Within this general framework, however, it is clear that the subtypes and density of voltage-gated ion channels in the AIS vary considerably [3,4], contributing to the diversity in spike shapes displayed by different neuron classes [5]. Action potential threshold also depends critically on the length and diameter of the AIS [6], as well as the spatial pattern of expression of voltage-gated ion channels [7,8].

The AIS is plastic: changes in both the length and distance of the AIS from the soma can be triggered in response to sustained changes in the level of synaptic excitation, resulting in compensatory alterations in spike threshold that maintain firing frequency within a neuron's dynamic range [9,10]. Voltage-gated calcium channels in the AIS have been shown to be important components of the modulatory control of spike initiation. Both T- and R-type voltage-gated calcium channels are expressed in the AIS of several types of neurons, where they may increase the probability of single spikes or contribute to burst firing [11]. In auditory brainstem neurons, dopamine down-regulates T-type channels through a protein kinase C pathway [12]. In dentate gyrus granule cells, acetylcholine reduces spike threshold through activation of muscarinic acetylcholine receptors, enhanced calcium influx in the AIS via T-type calcium channels, and reduction of Kv7 (M-type) potassium currents [13]. Thus, AIS calcium channels and G-protein coupled receptors provide mechanisms by which the sensitivity of spike generation can be finely tuned.

We have examined action potential initiation in the principal neurons of the medial superior olive (MSO), where control of spike threshold critically influences the processing of cues used for horizontal sound localization. [14]. Here we show that HCN channels are expressed in the AIS of MSO principal neurons, and that the primary role of these axonal channels is to alter action potential threshold, in contrast to the roles of somatic and dendritic channels on shaping the timing and summation of synaptic potentials. Additionally, we show that axonal HCN channels and their influence on spike threshold are subject to long-lasting modulation by serotonin through 5-HT_{1A} receptors. As the activity of the serotonergic system reports changes in motivational state or attention, axonal HCN channels may provide a way for neurons to translate such state changes into adjustments in firing sensitivity.

Results

Immunostaining for HCN1 subunits in the AIS

To explore the structural bases underlying action potential initiation and control of threshold in MSO principal neurons, we immunostained sections of gerbil brainstem using antibodies against βIV spectrin, a prominent cytoskeletal scaffold restricted to the AIS and nodes of Ranvier [15] and HCN1 subunits. Although the highest densities of HCN1-containing channels were in the soma and dendrites of MSO neurons (**Fig. 1a**), we detected low densities of HCN1 channels in 37/91 (41%) AIS as well (Fig. 1b, arrowheads). In some instances, HCN1 channels extended beyond the end of the βIV spectrin-labeled AIS (**Fig. 1b**, arrow). In MSO neurons the AIS emanated directly from the soma, rather than a primary dendrite (**Fig. 1a**). Furthermore, immunostaining for βIV spectrin or PanNav (detects all Na channel isoforms) began immediately adjacent to the cell body and averaged 17.4 ± 0.3 μm (n=46) and 18.2 ± 0.5 μm (n=12) in length, respectively (**Figs. 1a, 1d, and 1f**; p=0.2). Intriguingly,

immunostaining with antibodies against Nav1.6 Na channels revealed a prominent gap, or reduction in immunoreactivity at the proximal end of the AIS, with the highest levels of Nav1.6 at the distal end (**Fig. 1c**, arrow); this distribution of Nav1.6 is reminiscent of that found in cortical pyramidal neurons and retinal ganglion cells [7,16]. Consistent with this reduction in Nav1.6 immunoreactivity at the proximal AIS, we measured a shorter AIS length when defined by Nav1.6 immunoreactivity (**Fig. 1f**; 15.6 ± 0.5 μm, n=22; p=0.0062 for βIV spectrin length vs. Nav1.6 length and p=0.0016 for PanNav length vs. Nav1.6 length [unpaired t test with Welch's correction]). In some neurons, the distal end of the AIS also corresponded to the start of myelination, as indicated by immunostaining for the paranodal axoglial junction marker Caspr (**Fig. 1e**). Together, these results reveal molecular and structural details of the AIS of MSO neurons including the presence of HCN1 channels.

Function of HCN channels in the AIS using photoswitches

To investigate the expression and functional roles of HCN channels in the AIS, we combined confocal microscopy, electrophysiology, and optical manipulation of photoswitches, photoisomerizable compounds that can block the pore of certain voltage-gated ion channels in a wavelength-dependent fashion (**Fig. 2a**) [17]. To directly measure the biophysical properties of HCN channels in the AIS, we made whole-cell voltage-clamp recordings in MSO neurons from gerbils 18-23 postnatal days old, and isolated I_h pharmacologically (**Fig. 2b and Methods**). In these experiments we used DENAQ, which photoswitches to the *cis* (unblocking) configuration with 488 nm light and spontaneously reverts to the *trans* (blocking) configuration in darkness (**Supplementary Fig. 1**). In the dark DENAQ does not block I_h with 100% efficiency, yielding reduced currents in response to voltage steps (1s duration) from –30 mV to –110 mV in –10 mV increments ($I_{h,Dark}$: black traces; 1s prepulse to –30 mV; **Fig. 2c**). When the AIS was scanned with 488 nm light, DENAQ block of voltage-gated channels is relieved and the I_h in the AIS is augmented ($I_{h,488nm}$: green traces; **Fig. 2c**). Subtraction of the $I_{h,488nm}$ from $I_{h,Dark}$ yielded I_h isolated from the AIS ($I_{h,AIS}$; **Fig. 2d**). Tail current analysis of $I_{h,AIS}$ yielded a half-maximal activation voltage ($V_{½}$) of –64.4 ± 2.6 mV, with a slope of 10.0 ± 0.8 (n=6; **Fig. 2e**). These values were not significantly different from those obtained with somatic block (**Fig. 2e**; $I_{h,Soma}$: $V_{½}$ = –65.7 ± 2.9 mV, slope = 8.7 ± 0.9, $V_{½}$, p = 0.74; Slope, p = 0.16; n = 6). Finally, the activation kinetics of $I_{h,AIS}$ and $I_{h,Soma}$ (which exhibited both fast and slow time constants, τ_{fast} and τ_{slow}) were not significantly different from one another, nor was the relative proportion of these components to the total current amplitude **(Fig. 2f)**. These findings confirm the presence of I_h in the AIS of MSO cells, and also show that these channels display many of the same biophysical properties as those found throughout the rest of the cell.

To understand the functional roles of HCN channels in the AIS, we performed experiments with whole-cell current clamp recordings with AAQ. AAQ was maintained in its *cis*-conformation with field illumination at 380 nm, which maintains channels in an unblocked state (**Fig. 3a**). Local channel blockade was achieved by scanning either the AIS, soma, or whole cell with the confocal microscope's 488 nm laser line (**Fig. 3b**). A family of simulated EPSCs (sEPSCs) was injected through the patch pipette (0 to 4000 pA, 800 pA increment), giving rise to simulated postsynaptic potentials (sEPSPs) and typically action potentials in response to stronger stimuli (**Fig. 3b**, far left traces). Light-regulated channel blockade of the

AIS, soma and whole cell reversibly hyperpolarized the membrane resting potential (**Fig. 3b and 3c, gray bars)**. However, changes in resting potential were blocked completely when ZD7288 (20 μM), a non-photosensitive blocker of HCN channels, was included in the patch pipette solution (**Fig. 3c**, internal ZD7288**)**. AAQ is known to block multiple channel types, raising the possibility that nonspecific actions contribute to light-induced changes in resting potential. Bath application of 10 μM ZD7288 or 2 mM CsCl hyperpolarized MSO cells by an average of 6-7 mV when AAQ was maintained in the unblocked configuration under 380 nm illumination (**Fig. 3c**, bath ZD7288 and Cs^+). However, after restoration of the resting potential to control values via direct current injected through the pipette, no significant changes in resting potential occurred with 488 nm scanning of either the whole cell or AIS (**Fig. 3c)**. Finally, 5 μM XE-991, a blocker of KCNQ potassium channels that are present in the AIS of some cell types, did not significantly alter the resting potential (Ctl: –54.1 ± 1.1 mV; XE-991, –55.0 ± 1.0 mV; p=0.21; n=6; data not shown). Thus the action of AAQ on the resting potential is not explained by its action on other voltage-gated ion channels.

AAQ-mediated changes in the resting potential under 488 nm illumination were restricted to the AIS: in a subset of cells with planar axons over 100 μm in length, 488 nm light was scanned in each of three ROIs drawn over the axon in 30 μm increments (**Fig. 3d**). Significant light-activated changes in the resting potential were only generated in the proximal compartment encompassing the AIS (**Fig. 3e**; 0-30 μm, p=0.004; 30-60 μm, p=0.23; 60-90 μm, p=0.69; n=5), consistent with the expression of HCN1 subunits detected within and just beyond the distal end of the AIS (**Fig. 1**).

To address the functional influence of HCN channels in the AIS on action potential initiation we used AAQ to provide focal block of the AIS or soma during trains of synaptic stimuli delivered to either contralateral or ipsilateral excitatory inputs. In these experiments, GABAergic and glycinergic inhibitory inputs to MSO were blocked by 1 μM strychnine and 5 μM gabazine. The stimulation level was adjusted to generate approximately a 50% probability of spiking in control conditions (**Fig. 4a,b**, purple). Interestingly, when HCN channels in the AIS were blocked (**Fig. 4a**, green), spike probability increased over a broad range of frequencies (100 Hz: 30 ± 10.7 %, 200 Hz: 20 ± 6.9 %, 300 Hz: 11 ± 3.6 %, 400 Hz: 19 ± 8.0 %; n=4; **Fig. 4c**). By contrast, blocking HCN channels in the soma decreased spike probability (100 Hz: –26 ± 3.0 %, 200 Hz: –29 ± 14.6 %, 300 Hz: –30 ± 6.8 %, 400 Hz: –49 ± 15.8 %; n=4; **Fig. 4c**). When the shape of action potentials elicited under these conditions was examined with phase plane analysis (**Fig. 4d,e**, bottom), the maximum rate of rise of the action potential increased by 25% during AIS blockade (86.8 ± 7.5 mV/ms to 109.3 ± 13.5 mV/ms, p = 0.03), but only 9% during somatic blockade (79.8 ± 5.7 mV/ms to 86.9 ± 6.2 mV/ms, p = 0.06). In addition, the voltage threshold for action potentials was more significantly hyperpolarized during AIS blockade (−1.7 ± 0.4 mV, p = 0.03) than for somatic blockade (−0.4 ± 0.3, p = 0.24). The effects of somatic photoswitch blockade on spike probability and shape could be offset completely when light-induced changes in resting potential were compensated by depolarizing current injected through the recording pipette (**Supplementary Fig. 2**). In addition, using somatic current injection, changes in both spike threshold and maximum dV/dt could be induced in the soma but required strong hyperpolarization of the membrane potential (≥6 mV; **Supplementary Fig. 3**).

Additional experiments confirmed the involvement of HCN channels in controlling spike probability. In whole-cell current clamp recordings we generated trains of action potentials at 100 Hz with simulated EPSCs (0 to 6000 pA in 400 pA increments) and then applied brief puffs of either 50 μM ZD 7288 or a NaCl-based vehicle focally to the AIS or soma (**Fig. 5a-c**). In these experiments, the axon was visualized as before with confocal imaging of Alexa-568, and the spread of ZD7288 was visualized by monitoring the spread of fast green (1%), included in the puffing solution. The first spike among responses was analyzed for the comparison. When ZD7288 was applied to the AIS, the resting membrane potential of MSO neurons was significantly hyperpolarized (ZD7288: −1.8 ± 0.3 mV, $p = 0.007$; n=5; Veh.: −0.01 ± 0.2 mV, $p = 0.77$; n=3) and the shape of spikes changed (**Fig. 5b, upper panel; Fig. 5d**). In addition, the phase plane analysis clearly showed that the voltage threshold for action potentials was hyperpolarized (ZD: −2.58 ± 0.52 mV, $p = 0.008$; Veh.: −0.04 ± 0.22 mV, $p = 0.88$) and the maximum rate of rise increased (ZD: 30.62 ± 7.47 mV/ms, $p = 0.01$; Veh.: −1.25 ± 1.57 mV, $p = 0.51$) during ZD7288 application to the AIS (**Fig. 5b, lower panel, Fig. 5d, right)**. Focal application of ZD7288 to the side of the soma opposite to the AIS yielded comparable changes in the resting potential (ZD: −1.4 ± 0.31 mV, $p = 0.01$; n=5) but did not significantly alter the threshold (ZD: 0.20 ± 0.08 mV, $p = 0.08$) or maximum rate of rise (ZD: −1.08 ± 2.73 mV/ms, $p = 0.71$) of the action potential (**Fig. 5c,d)**. The fact that local pharmacological blockade of HCN channels mimics the compartment-specific effects of photoswitches indicates that the effects of AAQ on resting potential, spike threshold and spike shape are due to its blockade of HCN channels.

Modulation of HCN channels by serotonin

HCN channels are known to be the target of numerous modulatory neurotransmitters. Given the strong influence of HCN channels in the AIS on spike initiation, we asked whether modulation of these channels could influence action potential firing. The MSO receives a dense network of serotonergic fibers arising from the dorsal raphe nucleus [18,19]. To examine whether serotonin influences the properties of HCN channels, we made whole-cell voltage clamp recordings from MSO neurons, and isolated I_h pharmacologically (**Fig. 6a and Methods**). When 5-HT (300 μM) was continuously applied to the axon, soma and proximal dendrites of MSO neurons via a second patch pipette, the activation range of I_h was significantly shifted in the hyperpolarizing direction (−60.56 ± 1.96 mV to −71.25 ± 2.34 mV, $\Delta V_{1/2}$ = −10.69 ± 0.67 mV, p = 1.8E−05; n=6; **Fig. 6a,c,h**). While instantaneous leak current was stable in the presence of 5-HT (ΔInst. Leak = −3.75 ± 11.93 pA, $p = 0.77$, n=6), the maximum I_h was rapidly and significantly reduced (ΔMax. I_h = −119.39 ± 39.37 pA, $p = 0.02$; n=6; **Fig. 6b,g**). Application of 5-HT also increased both the fast and slow activation time constants of I_h while increasing the relative proportion of total current made up by the slow component (**Fig. 6i)**. The slow component likely reflected the presence of HCN4 subunits in MSO I_h: experiments in which block of I_h by the heart-slowing drug ivabradine was relieved for a component of I_h at negative voltages, a property of channels containing HCN4 but not HCN1 subunits **(Supplementary Fig. 4)**. In the presence of 10 μM WAY 100135, a 5-HT_{1A} antagonist, the modulatory effects of 5-HT on both the amplitude and activation voltage of I_h were eliminated (ΔV ½ = –1.44 ± 0.29 mV, p=0.07; ΔMax. I_h = –6.46 ± 18.68 pA, p=0.74; ΔInst. Leak = 27.32 ± 16.66 pA, p=0.45; n=7; **Fig. 6d-h**). WAY 100135 also strongly attenuated the 5-HT mediated increase in both activation time

constants (though τ_{fast} was still significantly increased vs. control), and eliminated significant changes in the relative amplitudes of τ_{fast} and τ_{slow} **(Fig 6i)**. The effects of 5-HT were reversible. In experiments with bath application of 20 μM 5-HT, the amplitude of I_h was reduced and the $V_{1/2}$ was negatively shifted as with local 5-HT applications, and these effects reversed within ~40 minutes (**Supplementary Fig. 5**). In addition to 5-HT_{1A} receptors, 5-HT_2 receptors have been reported to negatively shift the activation voltage of HCN channels. However, application of ketanserin (10-50 μM), a 5-HT_2 antagonist, did not alter 5-HT induced changes in either maximal current amplitude or activation voltages in I_h ($\Delta V½$ = –11.00 ± 2.08, p = 0.013, ΔMax. I_h = –157.58 ± 15.68 pA, p = 0.002; n=4, data not shown).

To understand whether the modulation of HCN channels by 5-HT affects action potential initiation through a local action in the axon, we made whole-cell current clamp recordings from MSO neurons and focally applied 5-HT (300 μM) to either the AIS or soma. Application of 5-HT to the AIS hyperpolarized the membrane potential (−1.29 ± 0.04 mV, p = 0.001; n=7), decreased spike threshold (ΔThreshold = −2.29 ± 0.44 mV, p = 0.002; n=7) and increased the maximum rate of rise of action potentials (121.21 ± 2.20 mV/ms, p = 0.002, n=7) (**Fig. 7a-d**). However, these effects were insignificant when 5-HT was applied to the AIS during recordings in which HCN channels had been blocked by internal application of 20 μM ZD 7288 through the recording pipette (Δ Vrest, −0.03 ± 0.13 mV/ms, p = 0.82; ΔThreshold, −0.08 ± 0.22 mV, p = 0.78; ΔMax dV/dt, −0.34 ± 3.3 mV/ms, p = 0.84; n=5). Finally, focal application of 5-HT to the soma produced changes in the resting potential but no significant changes in spike threshold or maximum dV/dt, highly similar to the focal blockade of HCN channels by focal ZD7288 (**Fig. 7c,d**; ΔVrest, −1.60 ± 0.20 mV, p = 0.01; ΔThreshold, −0.20 ± 0.08 mV, p = 0.08; ΔMax dV/dt, 1.08 ± 2.73 mV/ms, p = 0.71; n=6).

To address whether serotonin-induced modulation of spiking can be achieved by physiologically relevant concentrations of serotonin, during current-clamp recordings we electrically stimulated the plexus of serotonergic axons in and around the MSO while blocking AMPA, NMDA, GABA-A, and glycine receptors with NBQX (10 μM), AP-5 (50 μM), gabazine (5 μM) and strychnine (1 μM) respectively. Simulated EPSCs were injected through the somatic recording pipette every minute for 5 minutes, and both the resting potential and action potentials were monitored (**Fig. 8a-d**, Control condition). Recordings were discontinued if the resting membrane potential was not maintained within ± 1 mV for 5 minutes. In these experiments, a train of 50 stimuli at 200 Hz triggered small membrane depolarizations (less than 1 mV) that rose and decayed over hundreds of milliseconds and lacked discrete synaptic events. These slow depolarizations were reduced on average by 85% in the presence of 100 μM granisetron, an antagonist of ionotropic 5-HT_3 receptors (**Fig. 8b**; Ctl: ΔVm, 0.53 ± 0.05 mV, n=8; granisetron: ΔVm, 0.06 ± 0.03 mV, *p = 1.9E−05;* n=6), suggesting that these events represent the paracrine release of serotonin throughout the slice acting on ionotropic receptors. Correlated with this electrophysiological correlate of stimulated serotonin release, we observed robust and more long-term hyperpolarization of both the resting membrane potential and spike threshold. (**Fig. 8c,d**). Changes in resting potential and spike threshold lasted for the duration of recordings (tens of minutes), and were blocked by 68% and 95%, respectively, in the presence of 0.1 μM WAY 100135

(ΔVrest, −1.54 ± 0.31 mV, p = 0.0039; ΔThreshold: 0.19 ± 0.62 mV, $p = 0.81$; n=8) or when recordings were made with 20 μM internal ZD7288 to block HCN channels (ΔVrest, −0.66 ± 0.45 mV, $p = 0.40$; ΔThreshold, 0.19 ± 0.49 mV, $p = 0.56$; n=8). Together these results indicate that physiologically released serotonin is capable of triggering robust changes in the resting potential and action potential threshold of MSO neurons.

Discussion

In most neurons the AIS represents the final stage of synaptic integration, where the complex interplay between excitatory and inhibitory synaptic signals and voltage-gated ion channels determines whether the neuron generates an all-or-none action potential and successfully forwards its signal to its network targets. Action potential initiation sometimes has been regarded as static, exhibiting a discrete and constant threshold. Here we show in auditory neurons in the sound localization circuitry that HCN channels are expressed in the AIS, and by their proximity to the voltage-gated Na and K channels mediating action potential generation, regulate spike threshold through their influence on the local resting potential. We further show that modulation of I_h by serotonin can modify spike threshold through activation of 5-HT_{1A} receptors. Thus HCN channels in the AIS are in a position to adjust neural spike sensitivity in response to changes in motivation or state of attention.

The AIS of MSO neurons and the expression of HCN subunits

Action potential amplitude is unusually small in MSO principal neurons (5-20 mV), and yet immunolabeling for markers of the AIS show that the AIS is in fact only 12-22 μm long and emerges directly from the soma with no intervening gap (Fig. 1), in strong agreement with previous studies from MSO neurons [20] and their avian analogs in low frequency regions of the nucleus laminaris [6]. Interestingly, in MSO neurons immunolabeling of Nav 1.6 subunits was either reduced or absent in the region of the AIS nearest the soma, similar to results from retinal ganglion cells and prefrontal cortical neurons [7,16]. The distal bias of Nav1.6, together with the high percentage of inactivated Na channels at the soma [21] may both contribute to the electrical isolation of the AIS spike generator from the soma and dendrites. The expression of HCN1 subunits both in the AIS and slightly distal to the AIS extends previous studies that have shown enrichment of this subunit in the soma and dendrites of MSO neurons [22-24]. HCN4 (but not HCN2) subunits are also expressed in the soma and dendrites [22], but we did not detect the expression of HCN4 subunits in the AIS with antibody labeling (data not shown). Our electrophysiological evidence supports the presence of HCN4 subunits in the axon, however. MSO I_h isolated in the axon or soma exhibited the same dual activation time constants on time scales of tens and hundreds of milliseconds (**Fig. 2f, 6h**), consistent with the respective kinetics of HCN1 and HCN4 homomeric channels [25]. MSO I_h exhibits high sensitivity to cAMP, which binds to a cytoplasmic cyclic nucleotide binding domain, accelerating channel opening and shifting the activation range to more depolarized voltages [26]. The activation range of MSO I_h was shifted ~ –10 mV by modulation of cAMP levels through 5-HT1A receptors, a result more consonant with the presence of HCN4 subunits, which exhibit ~2-4 fold higher cAMP sensitivity than HCN1 subunits [26,27]. A component of MSO I_h recovered from block by ivabradine at negative voltages, a feature that differentiates HCN4 from HCN1 homomeric channels [28]. Although

we only detected HCN1 subunits in 41% of sampled MSO axons, 100% of photoswitch experiments revealed I_h in the axon. Thus, the complete lack of HCN4 labeling and inconsistent HCN1 labeling in MSO axons probably reflects limits in the sensitivity of the respective antibodies to the relatively low densities of HCN channels in the AIS relative to the soma and dendrites.

Action of Photoswitches on HCN channels

MSO neurons express KCNA1 (Kv1) channels at high density. Given that AAQ is known to block several subtypes of voltage-gated K channels in accordance with its quaternary ammonium group [17,29], it is perhaps surprising that the dominant effect of AAQ is predominantly on HCN channels. However, AAQ is an open channel blocker, and given that the average resting potential of MSO neurons resides at the foot of the Kv1 channel activation curve [30], the fraction of Kv1 channels active at rest is small relative to that of HCN channels [22,31]. Accordingly, photoswitching AAQ in 488 nm light had no significant effect on resting membrane potential, spike threshold or spike probability when HCN channels were first blocked pharmacologically (**Fig. 3c, Fig. 5, Supplementary Fig. 6**).

The regulation of spike threshold by HCN channels

HCN channels expressed in the soma and dendrites have been shown to play critical roles in synaptic integration: they shape temporal summation [32-34], and contribute to resonance in firing activity in both cortical and hippocampal neurons during network oscillations [35,36]. In auditory neurons concerned with preserving submillisecond timing information, including MSO principal neurons, HCN channels provide tonic membrane shunting, enabling fast-rising, precisely timed synaptic events [22,31,37]. By contrast, in the AIS, we found that HCN channels specifically reduced the probability of action potential firing (**Fig. 4**). Presumably this is mediated in part by an increase in Na channel inactivation in the AIS, consistent with the increase in rate of rise of the action potential during AIS-targeted HCN channel blockade. It is also possible that activation of KCNA1 (Kv1) channels, which are enriched in the AIS of both auditory and non-auditory neurons [8,38], may also activate through HCN channel activity, decreasing spike probability.

Interestingly, while hyperpolarizations of the resting potential occurred with blockade or neuromodulation of HCN channels at both the soma and AIS, reduction in spike threshold was far more sensitive to HCN channel manipulations in the AIS (**Supplementary Fig. 3**). Cable properties of the axon vs. the soma and dendrites may at least partially account for this disparity. Even modest amplitudes of I_h may produce large local voltage changes in the relatively small diameter AIS (~0.5 μm), but the voltage at the soma would be expected to undergo strong attenuation from the unusually large capacitive load imposed by the soma and large caliber dendrites as well as strong shunting arising from their unusually high levels of resting conductances [22]. Additionally, the observations above may also reflect local differences in the density and/or properties of voltage-gated ion channels in the two compartments [7,11,39].

Serotonergic modulation of HCN channels in the AIS

Within the central nervous system (CNS), the serotonergic projections from the raphe nuclei ramify widely throughout the brain [40], and include a dense projection to the MSO and other auditory brainstem nuclei [18,19]. We found that serotonin modulates of HCN channels in MSO neurons via 5-HT_{1A} receptors, which are coupled to the G proteins (G_i/G_o) that inhibit adenylyl cyclase and decrease cyclic adenosine monophosphate (cAMP) concentration [41]. Application of serotonin to whole MSO neurons decreased I_h, hyperpolarized the activation range by ~10 mV and slowed the activation/deactivation kinetics of the channels (**Fig. 6**), consistent with a decrease in adenylate cyclase activity and reduction in the allosteric modulation of I_h by cAMP [22,42]. Significantly, activation of 5-HT_{1A} receptors by serotonin released by stimulation of serotonergic fibers around the MSO hyperpolarized the resting potential and spike threshold through modulation of HCN channels (**Fig. 8a-d**), reflecting the local action of serotonin both on the soma and dendrites as well as the AIS (**Fig. 7a-c**). In neurons from the spinal cord and prefrontal cortex, the action of serotonin has been shown to decrease action potential firing through a modulatory decrease in voltage-gated Na current in the AIS [43,44]. However, we observed no serotonin-mediated changes in spike amplitude or shape in our experiments, inconsistent with effects on voltage-gated Na channels. In MSO neurons, the release of serotonin, as reported by voltage changes produced by co-activation of ionotropic 5-HT_3 receptors, increased and decayed over hundreds of milliseconds to seconds, consistent with a paracrine release mechanism observed in spinal cord and other auditory brainstem neurons [43,45].

Functional Implications

The serotonin-induced decrease in resting HCN channel conductance in the AIS lowers spike threshold without strongly affecting the membrane potential of the soma and dendrites. AIS calcium channels have also been shown to affect both spike probability and pattern, and these influences too can be altered through modulation [11,12]. These results highlight the critical role played by modulatory influences on voltage-gated ion channels in shaping both the probability and pattern of action potentials in the AIS. The functional influence of I_h modulation in the AIS bears some similarity to the effects of blocking AIS-targeted inhibitory inputs in cortical sensory neurons, where response levels increase additively, widening tuning curves without affecting their position [46,47]. In MSO neurons and their avian analogs, reduction of I_h in the soma and dendrites through modulation or pharmacological blockade has been shown to widen interaural time difference curves *in vitro* [22,48]. In these studies the reduction in I_h in the soma and dendrites degrades temporal resolution, presumably through an increase in input resistance and membrane time constant. The current findings show that some of these effects may also have contributions from local modulation of spike initiation in the AIS. Recent studies of synaptic integration in MSO neurons *in vitro* and *in vivo* have underscored the exquisite sensitivity of MSO spike initiation to small changes in resting potential [49,50], and thus even subtle modulatory influences on the resting potential and spike probability would have a significant impact on sensory coding.

Methods

All procedures were conducted in accordance with The University of Texas at Austin Institutional Animal Care and Use Committee, following guidelines of the National Institutes of Health.

Immunostaining

Gerbil brains (P21) were acutely dissected and drop-fixed in ice cold 4% paraformaldehyde, pH 7.2, for 1 hour. Brains were then transferred to 20% sucrose in 0.1M PB overnight, and then transferred to 30% sucrose in 0.1M PB until sectioning. 40 μm thick coronal sections of brainstem were then cut on a cryostat and mounted on coverslips. Sections were then immunostained as described [51] using mouse antibodies against HCN1 (clone N70/28 NeuroMab), PanNav [52], or Caspr (clone K65/35 NeuroMab), and rabbit antibodies against βIV spectrin [53] or Nav1.6 [54]. AIS lengths were measured using Zeiss Zen software (Zeiss, Thornwood, NY) or Image J (NIH). For AIS lengths, the start and end of the AIS was defined as the point at which the immunoreactivity fell below 10% of the maximum fluorescence intensity along the AIS. Statistics were performed using GraphPad Prism.

Brainstem slice preparation

Mongolian gerbils (*Meriones unguiculatus*) of both sexes were obtained from Charles River Laboratories or bred at the Animal Resource Center of the University of Texas at Austin. Litters were group housed and kept on a 12/12 hour light/dark cycle. Gerbils (P18-P23) were anesthetized with isoflurane, decapitated and the brain rapidly removed in artificial cerebrospinal fluid (ACSF) at 32°C. ACSF was bubbled with 95% O_2/ 5% CO_2 and contained (in mM) 125 NaCl, 25 glucose, 25 $NaHCO_3$, 2.5 KCl, 1.25 NaH_2PO_4, 1.5 $CaCl_2$, 1.5 $MgSO_4$, pH 7.45. Horizontal or coronal sections containing the superior olivary complex were cut at a thickness of 200 μM with an oscillating tissue slicer (VT1200S; Leica), incubated at 35°C for at least 30 min, and then held at room temperature until recording. Selected brain slices were biased towards the middle of the dorso-ventral (tonotopic) axis. MSO neurons were identified by their location in the slice, morphology, and distinct electrophysiological characteristics as in previous studies [55,56].

Photoswitch experiments

Brainstem slices were pre-incubated at room temperature in the dark for 20-30 minutes with either 300 μM AAQ diluted in ACSF for current clamp recordings or 200 μM DENAQ in ACSF for voltage clamp recordings. Thereafter, photoswitch-free ACSF was used for recordings. AAQ and DENAQ were custom synthesized [7] from Jublilant Chemsys., Ltd, Uttar Pradesh, India. Recordings were performed within 1 hour of photoswitch incubation to avoid time-dependent changes in the concentration of photoswitches in the membrane. To visualize the axon, soma and dendrites of MSO neurons, 40 μM Alexa Fluor 568 hydrazide (Invitrogen, Carlsbad, CA) was included in patch pipette solutions, and allowed to dialyze into neurons for at least 5 minutes after establishing a whole-cell recording. Excitation of Alexa 568 was achieved using the 543 nm laser line from a 1 mW HeNe laser through the 40x objective of a fixed stage upright confocal microscope (Leica TCS SP5 II). Excitation at 568 nm did not affect the conformation of AAQ or the intrinsic membrane properties of

MSO neurons. Scan speed was 400 Hz (pixel dwell time 4.9 μs), and ROIs generally occupied ~250 and ~600 pixels for the AIS and soma, respectively.

Current-clamp electrophysiology and imaging with AAQ—All current-clamp recordings were performed at 35°C in ACSF unless otherwise noted. Recordings were made using heat-polished borosilicate patch pipettes (1.65 mm outer diameter; World Precision Instruments, Sarasota, FL), and had resistances of 3-5 MΩ in ACSF. The internal solution in patch pipettes contained the following (in mM): 115 potassium gluconate, 20 KCl, 10 sodium phosphocreatine, 10 HEPES, 0.5 EGTA, 4 MgATP, 0.3 NaGTP, and the pH adjusted to 7.3 with KOH. Recordings were made with a Dagan (Minneapolis, MN) BVC-700A amplifier in current-clamp mode. To focally block voltage-gated ion channels in restricted sub-regions of MSO neurons, we combined whole-cell recordings, confocal microscopy, and the use of AAQ in gerbil brainstem slices. After identifying the intact AIS using 568 nm scans under the confocal microscope, the cell was continuously illuminated with 380 nm light through the epifluorescence port of the microscope, which maintains AAQ in the *cis* (non-blocking) conformation. The AIS, soma, or whole cell was then scanned with 488 nm light driving AAQ in to the *trans* (blocking) conformation, while simultaneously discontinuing the 380 nm illumination and initiating data acquisition of electrophysiological responses to real or simulated synaptic stimuli. Since all of the effects of this "photoblockade" were rapidly reversible upon reintroduction of 380 nm light, electrophysiological responses under 380 nm and 488 nm illumination were interleaved to control both for time dependent concentration changes in AAQ in cell membranes and AAQ molecules entering a non-reversible configuration. Data acquisition was controlled by custom macros programmed in Igor Pro (WaveMetrics, Lake Oswego, OR).

The effective spatial resolution of photoswitches was assessed with AAQ. Using a 30 μm ROI over the AIS, we measured how the change in resting potential at 488 nm was affected by moving the ROI perpendicular to the long axis of the axon in 0.5 μm steps (**Supplementary Fig. 7**). The change in membrane potential decreased exponentially with a distance constant of 0.37 μm, close to the theoretical point spread function of 0.31 μm at 488 nm, demonstrating that the compartment-specific effects of AAQ blockade are minimally affected by light scattering in the slice. Recordings were only included if the series resistance was <20 MΩ. All reported membrane potentials recorded with KGluconate are corrected for a liquid junction potential of 10 mV.

Voltage-clamp electrophysiology and imaging with DENAQ—All voltage-clamp recordings were made in whole-cell configuration using an Axopatch 200B amplifier (Molecular Devices), filtered at 3 kHz and acquired to computer at 50 kHz via an Instrutech ITC-18 interface (Heka Instruments). Pipette solutions were identical to those in current-clamp recordings. Experiments were conducted at room temperature in ACSF. To reduce the effects of whole-cell dialysis on the activation voltage of HCN channels patch-pipettes had open tip resistances of between 4-5 MΩ (as in Khurana et al., 2012) and the time of data collection was limited to 15 minutes. Series resistance was compensated by at least 95% and pipettes were coated with Sylgard to reduce capacitance. For pharmacologically isolating I_h, the following was added to the external ACSF (in mM): 1 3,4-diaminopyridine (DiAP), 10

TEA-Cl, 0.2 4-aminopyridine, 0.2 $BaCl_2$, 0.001 TTX, 0.05 $NiCl_2$, 0.2 $CoCl_2$, 0.01 NBQX, 0.05 $_D$-AP5, and 0.001 strychnine. DENAQ exhibits the *cis* (unblocked) conformation in visible light (450-550 nm) and relaxes rapidly to the *trans* (blocked) conformation in the dark [58,59]. Thus, in DENAQ experiments cells were maintained in the dark in the blocked state and then I_h was unblocked by scanning regions of interest with the 488 nm laser. I_h in ROIs was revealed by subtracting I_h records in 488 nm illumination from those recorded in the dark. All reported membrane potentials recorded with KGluconate are corrected for a liquid junction potential of 10 mV.

Synaptic stimulation

Activation of synaptic inputs to MSO cells was performed by delivering brief (0.1 ms) electrical pulses to the slice through patch pipettes (tip diameter: 10 μm). Stimulation electrodes were placed either medial or lateral to the MSO, activating either contralateral or ipsilateral excitatory inputs from the cochlear nucleus, respectively. The probability of action potentials driven by synaptic excitation was not affected by illumination of AAQ in photoswitch experiments when light-induced changes in postsynaptic resting potential were offset with DC current, precluding significant presynaptic effects of AAQ (**Supplementary Fig. 2**).

Focal application of ZD7288 or 5-HT

The puffing solution contained the following (in mM): 10 glucose, 125 NaCl, 2.5 KCl, 3 HEPES, and 1% fast green for monitoring the spread of drugs. ZD7288 (50 μM) or 5-HT (300 μM) was included in the puffing solution. Initially, the AIS of MSO neurons was visualized through a confocal microscope prior to gentle application of either ZD7288 or 5-HT to the AIS.

Data analysis and statistics

All data analyses were performed using custom routines implemented in Igor Pro (Wavemetrics, Lake Oswego, OR). For voltage-clamp recording, MSO neurons were held at −60 mV, and then depolarized to –30 mV for 1 second to deactivate I_h. Subsequently, I_h was activated with voltage steps from −30 to −110 mV in 10 mV increments and followed by a 1 s step to −100 mV to elicit tail currents. Peak tail currents were averaged from the 10 ms immediately following the capacitive transient and normalized to minimum and maximum tail currents obtained from −110 mV and –30 mV prepulses, respectively. The activation range of HCN channels was quantified by plotting peak tail currents to maximum and minimum I_h and fitting this relationship to a Boltzmann equation of the form $f(V) = 1/(1+\exp[(V_{1/2}-V)/k])$, where V is the membrane voltage, $V_{1/2}$ is the half-maximal activation voltage, and k is the slope factor. Time constants of activation of I_h were measured using bi-exponential fits of tail currents in response to voltage steps from –30 mV to –110 mV. In all experiments, values are presented as mean ± SEM, and statistical significance was assessed using a two-tailed Student's t test or a two-way ANOVA for repeated measures at a significance level of 0.05 unless otherwise indicated. Data distribution was assumed to be normal but this was not formally tested. No statistical methods were used to predetermine

sample sizes but they were consistent with other publications in the field. Numbers of replications (n's) are equal to the number of animals used.

Supplementary Material

Refer to Web version on PubMed Central for supplementary material.

Acknowledgements

This work was supported by NIH grants NS044916 (M.N.R.), EY018957 (R.H.K.) and DC006788 (N.L.G.). The authors would like to acknowledge S. Khurana, who first observed that serotonin activates 5-HT3 receptors in MSO neurons.

Bibliography

1. Coombs JS, Curtis DR, Eccles JC. The interpretation of spike potentials of motoneurones. J Physiol. 1957; 139:198–231. [PubMed: 13492209]
2. Stuart GJ, Sakmann B. Active propagation of somatic action potentials into neocortical pyramidal cell dendrites. Nature. 1994; 367:69–72. [PubMed: 8107777]
3. Grubb MS, Shu Y, Kuba H, Rasband MN, et al. Short- and long-term plasticity at the axon initial segment. J Neurosci. 2011; 31:16049–16055. [PubMed: 22072655]
4. Yoshimura T, Rasband MN. Axon initial segments: diverse and dynamic neuronal compartments. Curr Opin Neurobiol. 2014; 27:96–102. [PubMed: 24705243]
5. Bean BP. The action potential in mammalian central neurons. Nat Rev Neurosci. 2007; 8:451–465. [PubMed: 17514198]
6. Kuba H, Ishii T, Ohmori H. Axonal site of spike initiation enhances auditory coincidence detection. Nature. 2006; 444:1069–1072. [PubMed: 17136099]
7. Hu W, Tian C, Li T, Yang M, et al. Distinct contributions of Na(v)1.6 and Na(v)1.2 in action potential initiation and backpropagation. Nat Neurosci. 2009; 12:996–1002. [PubMed: 19633666]
8. Kole MH, Letzkus JJ, Stuart GJ. Axon initial segment Kv1 channels control axonal action potential waveform and synaptic efficacy. Neuron. 2007; 55:633–647. [PubMed: 17698015]
9. Grubb MS, Burrone J. Activity-dependent relocation of the axon initial segment fine-tunes neuronal excitability. Nature. 2010; 465:1070–1074. [PubMed: 20543823]
10. Kuba H, Oichi Y, Ohmori H. Presynaptic activity regulates Na(+) channel distribution at the axon initial segment. Nature. 2010; 465:1075–1078. [PubMed: 20543825]
11. Bender KJ, Trussell LO. Axon initial segment Ca2+ channels influence action potential generation and timing. Neuron. 2009; 61:259–271. [PubMed: 19186168]
12. Bender KJ, Ford CP, Trussell LO. Dopaminergic modulation of axon initial segment calcium channels regulates action potential initiation. Neuron. 2010; 68:500–511. [PubMed: 21040850]
13. Martinello K, Huang Z, Lujan R, Tran B, et al. Cholinergic afferent stimulation induces axonal function plasticity in adult hippocampal granule cells. Neuron. 2015; 85:346–363. [PubMed: 25578363]
14. Grothe B. Sensory systems: New roles for synaptic inhibition in sound localization. Nat Rev Neurosci. 2003; 4:540–550. [PubMed: 12838329]
15. Berghs S, Aggujaro D, Dirkx R, Maksimova E, et al. betaIV spectrin, a new spectrin localized at axon initial segments and nodes of ranvier in the central and peripheral nervous system. J Cell Biol. 2000; 151:985–1002. [PubMed: 11086001]
16. Van Wart A, Trimmer JS, Matthews G. Polarized distribution of ion channels within microdomains of the axon initial segment. J Comp Neurol. 2007; 500:339–352. [PubMed: 17111377]
17. Mourot A, Tochitsky I, Kramer RH. Light at the end of the channel: optical manipulation of intrinsic neuronal excitability with chemical photoswitches. Front Mol Neurosci. 2013; 6:5. [PubMed: 23518818]

18. Hurley LM, Thompson AM. Serotonergic innervation of the auditory brainstem of the Mexican free-tailed bat, Tadarida brasiliensis. J Comp Neurol. 2001; 435:78–88. [PubMed: 11370012]
19. Thompson AM, Hurley LM. Dense serotonergic innervation of principal nuclei of the superior olivary complex in mouse. Neurosci Lett. 2004; 356:179–182. [PubMed: 15036624]
20. Lehnert S, Ford MC, Alexandrova O, Hellmundt F, et al. Action potential generation in an anatomically constrained model of medial superior olive axons. J Neurosci. 2014; 34:5370–5384. [PubMed: 24719114]
21. Scott, Mathews & Golding Perisomatic voltage-gated sodium channels actively maintain linear synaptic integration in principal neurons of the medial superior olive. J Neurosci. 2010; 30:2051–2062. [PubMed: 20147533]
22. Khurana S, Liu Z, Lewis AS, Rosa K, et al. An essential role for modulation of hyperpolarization-activated current in the development of binaural temporal precision. J Neurosci. 2012; 32:2814–2823. [PubMed: 22357864]
23. Koch U, Braun M, Kapfer C, Grothe B. Distribution of HCN1 and HCN2 in rat auditory brainstem nuclei. Eur J Neurosci. 2004; 20:79–91. [PubMed: 15245481]
24. Kopp-Scheinpflug C, Pigott BM, Forsythe ID. Nitric oxide selectively suppresses IH currents mediated by HCN1-containing channels. J Physiol. 2015; 593:1685–1700. [PubMed: 25605440]
25. Santoro B, Chen S, Luthi A, Pavlidis P, et al. Molecular and functional heterogeneity of hyperpolarization-activated pacemaker channels in the mouse CNS. J Neurosci. 2000; 20:5264–5275. [PubMed: 10884310]
26. Wainger BJ, DeGennaro M, Santoro B, Siegelbaum SA, Tibbs GR. Molecular mechanism of cAMP modulation of HCN pacemaker channels. Nature. 2001; 411:805–810. [PubMed: 11459060]
27. Ishii TM, Takano M, Xie L-H, Noma A, Ohmori H. Molecular Characterization of the Hyperpolarization-activated Cation Channel in Rabbit Heart Sinoatrial Node. Journal of Biological Chemistry. 1999; 274:12835–12839. [PubMed: 10212270]
28. Bucchi A, Tognati A, Milanesi R, Baruscotti M, DiFrancesco D. Properties of ivabradine-induced block of HCN1 and HCN4 pacemaker channels. J Physiol. 2006; 572:335–346. [PubMed: 16484306]
29. Kramer RH, Mourot A, Adesnik H. Optogenetic pharmacology for control of native neuronal signaling proteins. Nat Neurosci. 2013; 16:816–823. [PubMed: 23799474]
30. Mathews PJ, Jercog PE, Rinzel JR, Scott LL, Golding NL. Control of submillisecond synaptic timing in binaural coincidence detectors via a somatically directed gradient of Kv1 channels. Nat Neurosci. 2010; 13:601–609. [PubMed: 20364143]
31. Baumann VJ, Lehnert S, Leibold C, Koch U. Tonotopic organization of the hyperpolarization-activated current (Ih) in the mammalian medial superior olive. Front Neural Circuits. 2013; 7:117. [PubMed: 23874271]
32. Harnett MT, Magee JC, Williams SR. Distribution and function of HCN channels in the apical dendritic tuft of neocortical pyramidal neurons. J Neurosci. 2015; 35:1024–1037. [PubMed: 25609619]
33. Magee JC. Dendritic Ih normalizes temporal summation in hippocampal CA1 neurons. Nat Neurosci. 1999; 2:848. [PubMed: 10461231]
34. Poolos NP, Migliore M, Johnston D. Pharmacological upregulation of h-channels reduces the excitability of pyramidal neuron dendrites. Nat Neurosci. 2002; 5:767–774. [PubMed: 12118259]
35. McCormick DA, Pape HC. Properties of a hyperpolarization-activated cation current and its role in rhythmic oscillation in thalamic relay neurones. J Physiol. 1990; 431:291–318. [PubMed: 1712843]
36. Narayanan R, Johnston D. Long-term potentiation in rat hippocampal neurons is accompanied by spatially widespread changes in intrinsic oscillatory dynamics and excitability. Neuron. 2007; 56:1061–1075. [PubMed: 18093527]
37. Golding NL, Robertson D, Oertel D. Recordings from slices indicate that octopus cells of the cochlear nucleus detect coincident firing of auditory nerve fibers with temporal precision. J Neurosci. 1995; 15:3138–3153. [PubMed: 7722652]

38. Dodson PD, Barker MC, Forsythe ID. Two heteromeric Kv1 potassium channels differentially regulate action potential firing. J Neurosci. 2002; 22:6953–6961. [PubMed: 12177193]
39. Colbert CM, Pan E. Ion channel properties underlying axonal action potential initiation in pyramidal neurons. Nat Neurosci. 2002; 5:533–538. [PubMed: 11992119]
40. Steinbusch HW. Distribution of serotonin-immunoreactivity in the central nervous system of the rat-cell bodies and terminals. Neuroscience. 1981; 6:557–618. [PubMed: 7017455]
41. Polter AM, Li X. 5-HT1A receptor-regulated signal transduction pathways in brain. Cell Signal. 2010; 22:1406–1412. [PubMed: 20363322]
42. Wang J, Chen S, Nolan MF, Siegelbaum SA. Activity-dependent regulation of HCN pacemaker channels by cyclic AMP: signaling through dynamic allosteric coupling. Neuron. 2002; 36:451–461. [PubMed: 12408847]
43. Cotel F, Exley R, Cragg SJ, Perrier JF. Serotonin spillover onto the axon initial segment of motoneurons induces central fatigue by inhibiting action potential initiation. Proc Natl Acad Sci U S A. 2013; 110:4774–4779. [PubMed: 23487756]
44. Yin L, Rasch MJ, He Q, Wu S, et al. Selective Modulation of Axonal Sodium Channel Subtypes by 5-HT1A Receptor in Cortical Pyramidal Neuron. Cereb Cortex. 2015
45. Tang ZQ, Trussell LO. Serotonergic regulation of excitability of principal cells of the dorsal cochlear nucleus. J Neurosci. 2015; 35:4540–4551. [PubMed: 25788672]
46. Sturgill JF, Isaacson JS. Somatostatin cells regulate sensory response fidelity via subtractive inhibition in olfactory cortex. Nat Neurosci. 2015; 18:531–535. [PubMed: 25751531]
47. Wilson NR, Runyan CA, Wang FL, Sur M. Division and subtraction by distinct cortical inhibitory networks in vivo. Nature. 2012; 488:343–348. [PubMed: 22878717]
48. Yamada R. Hyperpolarization-Activated Cyclic Nucleotide-Gated Cation Channels Regulate Auditory Coincidence Detection in Nucleus Laminaris of the Chick. J Neurosci. 2005; 25:8867–8877. [PubMed: 16192376]
49. Franken TP, Roberts MT, Wei L, Golding NL, Joris PX. In vivo coincidence detection in mammalian sound localization generates phase delays. Nat Neurosci. 2015; 18:444–452. [PubMed: 25664914]
50. Roberts MT, Seeman SC, Golding NL. A mechanistic understanding of the role of feedforward inhibition in the mammalian sound localization circuitry. Neuron. 2013; 78:923–935. [PubMed: 23764291]
51. Chang KJ, Zollinger DR, Susuki K, Sherman DL, et al. Glial ankyrins facilitate paranodal axoglial junction assembly. Nat Neurosci. 2014; 17:1673–1681. [PubMed: 25362471]
52. Rasband MN, Peles E, Trimmer JS, Levinson SR, et al. Dependence of nodal sodium channel clustering on paranodal axoglial contact in the developing CNS. J Neurosci. 1999; 19:7516–7528. [PubMed: 10460258]
53. Yang Y, Lacas-Gervais S, Morest DK, Solimena M, Rasband MN. BetaIV spectrins are essential for membrane stability and the molecular organization of nodes of Ranvier. J Neurosci. 2004; 24:7230–7240. [PubMed: 15317849]
54. Schafer DP, Custer AW, Shrager P, Rasband MN. Early events in node of Ranvier formation during myelination and remyelination in the PNS. Neuron Glia Biol. 2006; 2:69–79. [PubMed: 16652168]
55. Mathews PJ, Jercog PE, Rinzel JR, Scott LL, Golding NL. Control of submillisecond synaptic timing in binaural coincidence detectors via a somatically directed gradient of Kv1 channels. Nat Neurosci. 2010; 13:601–609. [PubMed: 20364143]
56. Scott LL, Mathews PJ, Golding NL. Posthearing developmental refinement of temporal processing in principal neurons of the medial superior olive. J Neurosci. 2005; 25:7887–7895. [PubMed: 16135745]
57. Banghart MR, Mourot A, Fortin DL, Yao JZ, et al. Photochromic blockers of voltage-gated potassium channels. Angew Chem Int Ed Engl. 2009; 48:9097–9101. [PubMed: 19882609]
58. Mourot A, Tochitsky I, Kramer RH. Light at the end of the channel: optical manipulation of intrinsic neuronal excitability with chemical photoswitches. Front Mol Neurosci. 2013; 6:5. [PubMed: 23518818]

59. Tochitsky I, Polosukhina A, Degtyar VE, Gallerani N, et al. Restoring visual function to blind mice with a photoswitch that exploits electrophysiological remodeling of retinal ganglion cells. Neuron. 2014; 81:800–813. [PubMed: 24559673]

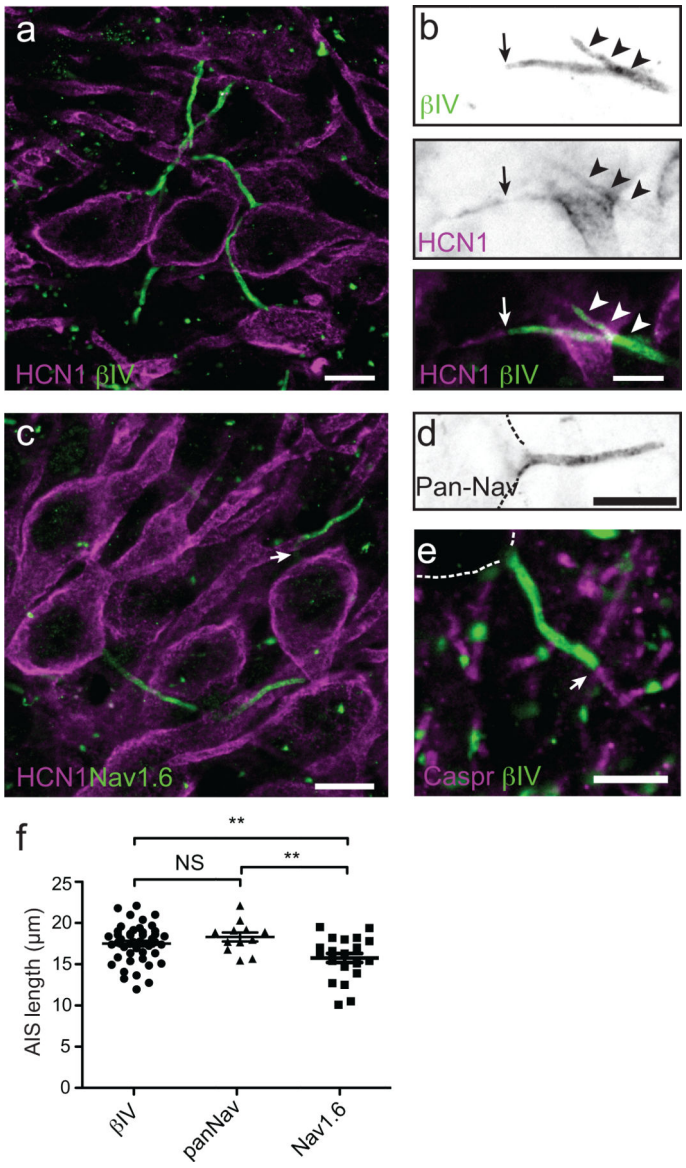

Figure 1. Expression of HCN1 subunits in the AIS of MSO principal neurons

(**a**) Immunostaining of MSO neurons using antibodies against HCN1 (red) and βIV spectrin (green). Scale = 10 um. (**b**) Immunostaining of MSO neuron AIS using antibodies against HCN1(red) and βIV spectrin (green). Arrowheads indicate HCN1 immunoreacitivity that colocalizes with βIV spectrin. The arrow indicates the end of the βIV spectrin-labeled AIS. HCN1 immunoreactivity frequently extended beyond the end of the AIS into the more distal axon. Scale = 5 um. (**c**) Immunostaining of MSO neurons using antibodies against HCN1 (red) and Nav1.6. Nav1.6 immunoreactivity frequently decreased in intensity or was absent immediately adjacent to the cell body (arrow). Scale = 10 um. (**d**) MSO neuron AIS immunostained using a Pan-specific Nav channel antibody (PanNav). This immunoreactivity began at the transition from the cell body to the axon. Dotted lines outline the cell body. Scale = 10 um. (**e**) Immunostaining of MSO using antibodies against caspr (red) and βIV spectrin (green). The arrow indicates the end of the AIS and the start of the myelin sheath.

Scale = 10 um. (**f**) length of βIV spectrin, PanNav, and Nav1.6 labeling along the AIS of MSO neurons. The length of Nav1.6-labeling was significantly less than either βIV spectrin or PanNav staining, reflecting the reduced staining near the cell body. βIV spectrin: n=46; PanNav: n=12; Nav1.6, n=22. βIV spectrin vs. PanNav: p=0.2; βIV spectrin vs. Nav1.6: p=0.006; PanNav vs. Nav1.6: p=0.001 (unpaired t-test with Welch's correction). Scatterplots show mean±SEM.

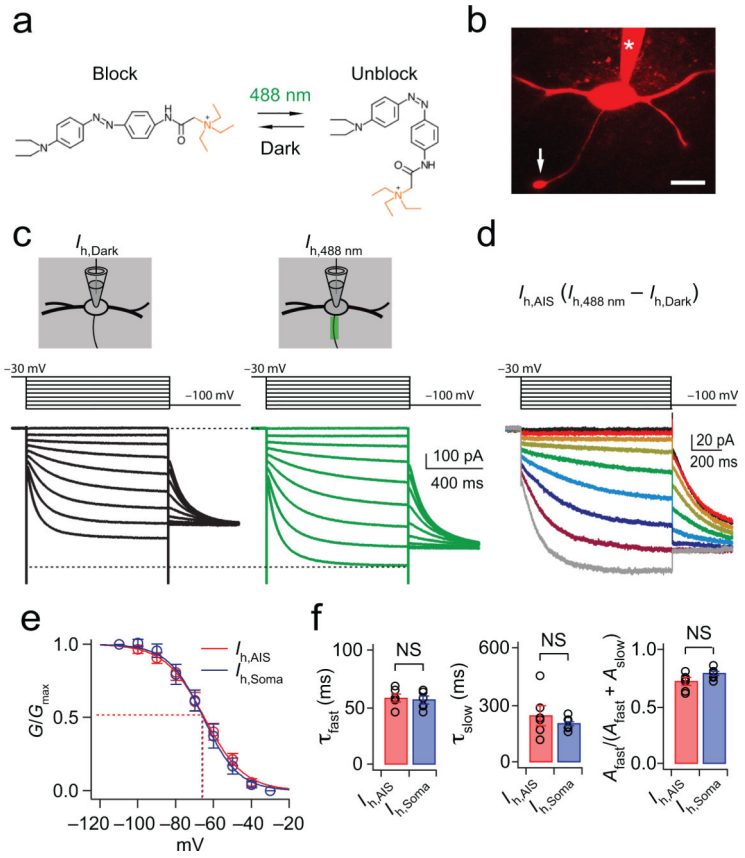

Figure 2. Activation properties of axonal I_h, as revealed by laser scanning of the photoswitch DENAQ

(a) The *cis*, unblocking conformation of DENAQ is maintained at 488 nm light (green) while the *trans*, blocking conformation is maintained in the dark (black). **(b)** Confocal image of an MSO principal neuron. Arrow: axon bleb; asterisk: patch pipette; scale = 30 μm. (**c**) Measurement of I_h in the AIS using DENAQ and whole-cell voltage-clamp recordings. Pharmacologically isolated I_h was partially blocked in the dark (black traces) and then focally unblocked in the AIS at 488 nm (green traces). Voltage steps: −30 mV to −110 mV in −10 mV steps, 1 s duration. (**d**) $I_{h,AIS}$ yielded from subtraction of $I_{h,Dark}$ (**c**, ***left***) from $I_{h,488nm}$ (**c**, ***right***) ($I_{h,AIS} = I_{h,488nm} - I_{h,Dark}$). Instantaneous tail currents measured at −100 mV. (**e**) The voltage dependence and slope of I_h in the AIS are not significantly different from those in the soma ($V_{½}$, $p = 0.74$; Slope, $p = 0.17$; n=6). 2-tailed, paired *t* test. (**f**) I_h in the axon and soma exhibit fast and slow exponential components, and each component in the two locations is statistically indistinguishable, as is the relative proportion of their current amplitudes (τ_{fast}, $p = 0.56$; τ_{slow}, $p = 0.33$; [$A_{fast}/(A_{fast}+A_{slow})$], $p = 0.08$; 2-tailed, unpaired *t* test. Error bars indicate SEM.

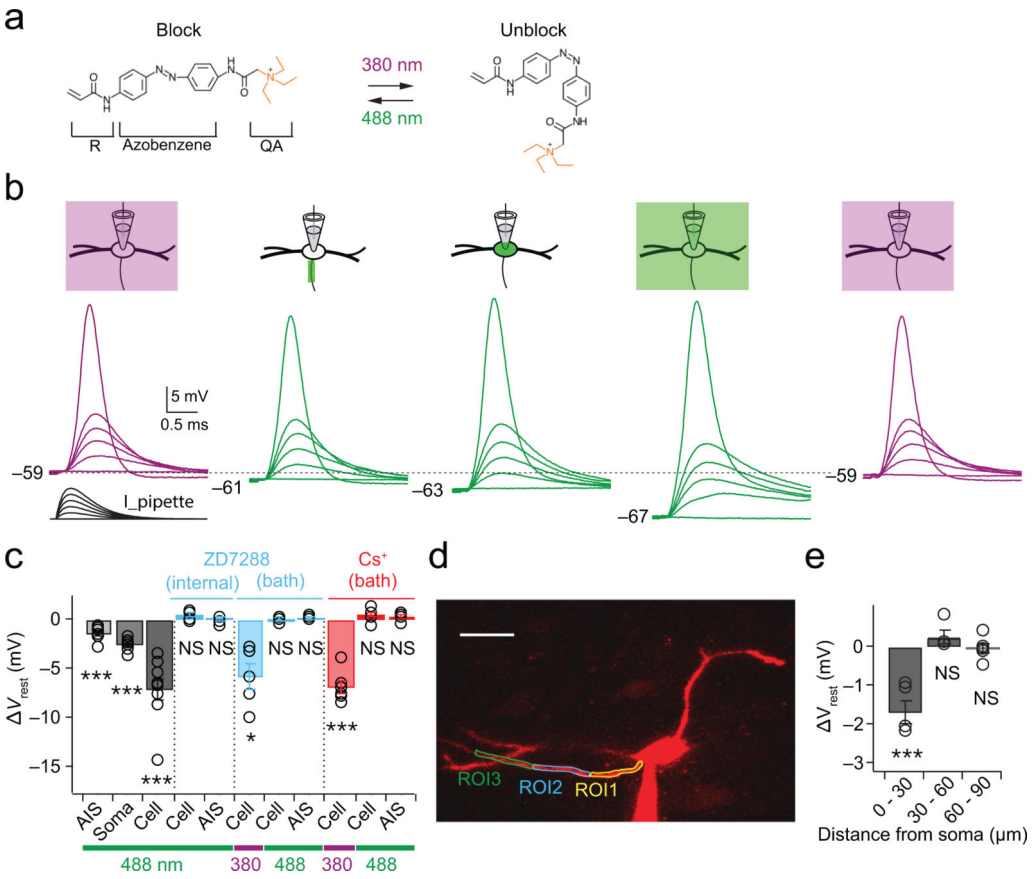

Figure 3. Compartment-specific block of resting conductances by laser scanning of AAQ

(**a**) The unblocking and blocking conformations of AAQ are maintained at 380 and 488 nm light, respectively. R, acrylamide group; QA, quaternary ammonium group. (**b**) Scanning block of different cellular compartments reversibly alters the resting potential and duration of responses to simulated EPSCs during whole-cell current-clamp recordings. Purple and green traces: unblocked and blocked conformations of AAQ, respectively. Simulated EPSCs: 0 – 4 nA, 0.8 nA steps. (**c**) Compartment-specific effects of 488 nm illumination of AAQ on resting potentials (grayscale bars; n=9). The resting potential is not altered by 488 nm scanning in the presence of the HCN channel blocker ZD7288 (20 μM) applied through the recording pipette (ZD7288, "Internal"; p=0.66 and 0.07 for cell and AIS; n=6). Block of HCN channels with external 10 μM ZD7288 or 2 mM CsCl hyperpolarizes the resting potential when AAQ is under 380 nm illumination, but after restoration of the membrane potential to control values with DC current, no further changes in voltage are induced with 488 nm scanning (ZD7288 "Bath", p = 0.015 for Cell at 380 nm, p = 0.08 and 0.86 for AIS and Cell at 488 nm, n=5; Cs^+ "Bath", p = 0.0001 for Cell at 380 nm, p = 0.24 and 0.13 for AIS and Cell at 488 nm, n=6). (**d**) Spatial dependence of photoswitch-induced changes in resting potential. Adjacent ROIs were 30 μm long. Scale bar, 30 μm. (**e**) Changes in resting potentials only occurred at in the proximal ROI overlapping the AIS (0-30 μm, p = 0.0035; 30-60 μm, p = 0.23; 60-90 μm, p = 0.69; n=5). Error bars indicate SEM. * p<0.05; *** p<0.01.

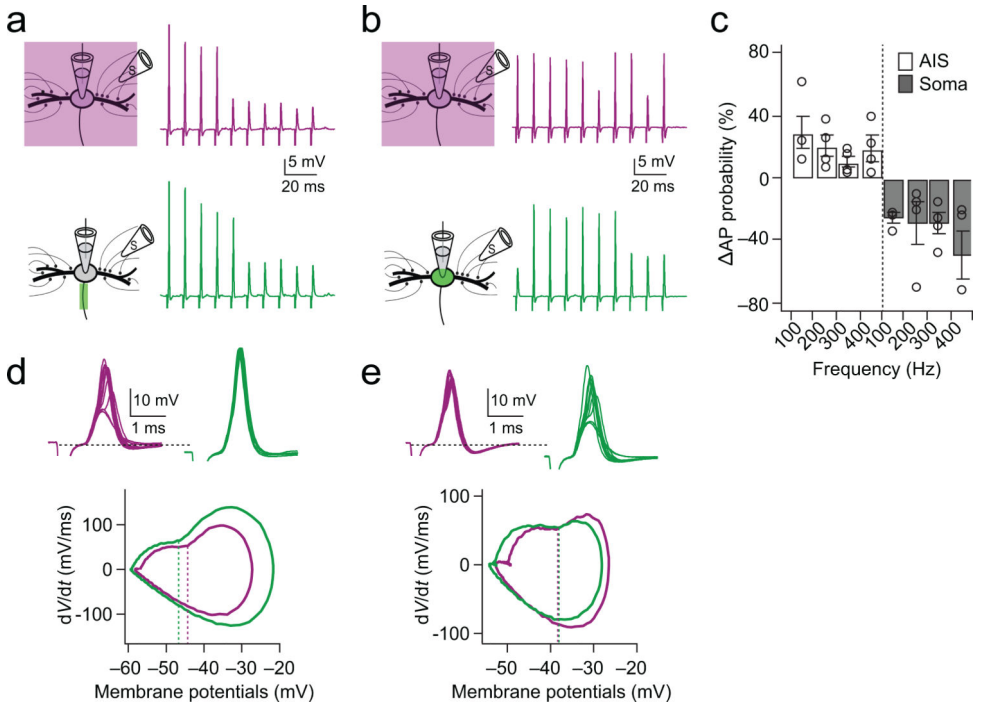

Figure 4. HCN channels in the AIS but not the soma and dendrites decrease spike probability by raising threshold

(a) Responses to synaptic stimulation during a whole-cell current clamp recording with AAQ maintained in the unblocked conformation with 380 nm field illumination (purple traces) and during AIS blockade of HCN channels with focal 488 nm illumination (green traces). *Left:* experimental configuration. *Right:* responses to contralateral train stimuli (100 Hz, 10 pulses). Vrest(380 nm) = –56 mV, Vrest(488 nm) = –58 mV. (**b**) In a different cell, identical protocol as in **a**, except that AAQ-induced blockade was induced in the soma. Vrest (380 nm) = – 58 mV, Vrest(488 nm) = –62 mV. (**c**) Group data showing that the change in spike probability increases during blockade of HCN channels in the AIS (open bars) but decreases during blockade of HCN channels of the soma (gray bars; n=4). (**d**) *Top:* The first responses to each of 10 stimulus repetitions are shown in **a**, superimposed. *Bottom:* Phase plane plot (averaged) of spikes initiated in the traces shown in upper traces. Dash lines represent the average voltage threshold of spikes in each condition. **(e**). Identical protocol as in **d**, except data from **b**.

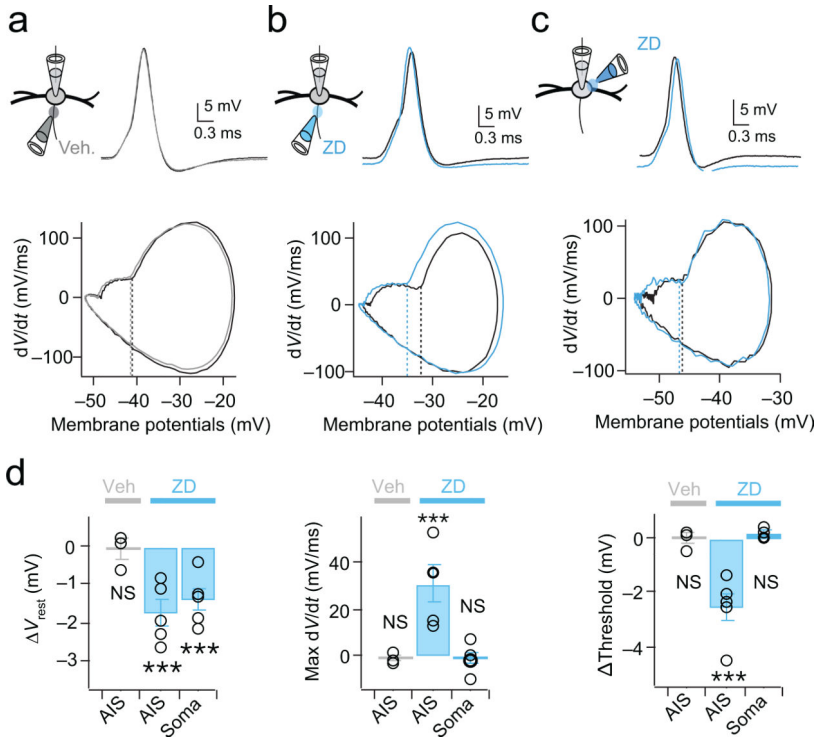

Figure 5. Local pharmacological blockade of HCN channels in the AIS mimics the effects of photoswitches

(**a**) *Top:* First suprathreshold spike in response to a train of somatic simulated EPSCs (100 Hz; 0-6 nA, 0.4 pA steps) in a whole-cell current clamp recording in control (black) and following brief focal pressure application of a NaCl-based vehicle onto the AIS (gray) *Bottom:* Phase plot of the first spike under each condition. Dotted lines: spike threshold. The vehicle (gray) alters neither the shape, maximum rate of rise (d*V*/d*t*), or threshold of spikes. Vrest = –59 mV for both control and vehicle. (**b**) Brief focal pressure application of 50 μM ZD7288 onto the AIS (blue) hyperpolarizes both the resting potential (*Middle*) and action potential threshold (phase plot, *middle*), and increases maximum d*V*/d*t* of the spike. Vrest = –52 mV (control), –54 mV (ZD7288). (**c**) Focal application of 50 μM ZD7288 to the soma on the opposite side of the AIS hyperpolarizes the resting potential but does not change the threshold or shape of the action potential. Vrest = –59 mV and –61 mV for control and ZD7288, respectively. (**d**) Group data quantifying average changes in resting membrane potential, voltage threshold and maximum rate of rise of spikes with focal ZD7288 blockade of HCN channels in the AIS (ΔVrest: Veh., p=0.77, ZD(AIS), p=0.07, ZD(Soma), p=0.01; ΔThreshold: Veh., p=0.88, ZD(AIS), p=0.008, ZD(Soma), p=0.08; ΔMax d*V*/d*t*: Veh., p=0.51, ZD(AIS), p=0.01, ZD(Soma), p=0.71; Veh, n=3; ZD, n=5). 2-tailed paired *t* test. Error bars indicate SEM. *** p<0.001

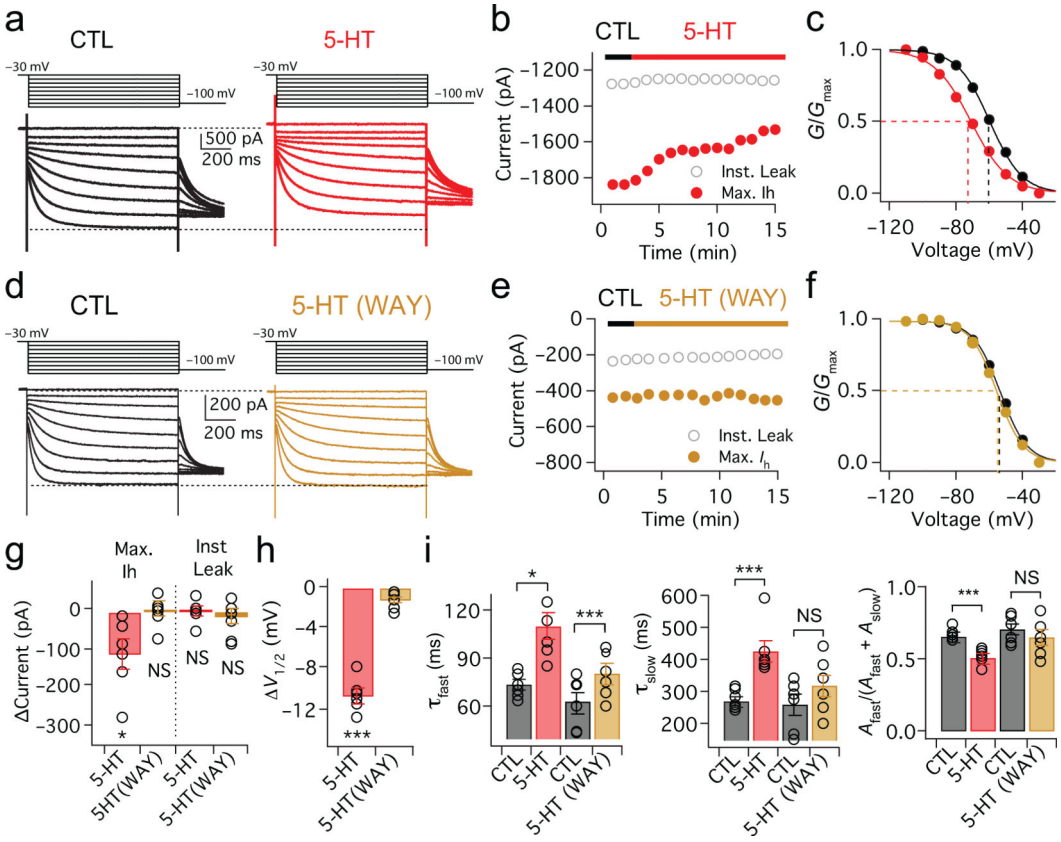

Figure 6. Serotonin modulates the activation range of HCN channels through 5-HT$_{1A}$ receptors

(**a**) Voltage dependence of I_h activation in whole-cell voltage-clamp recordings (voltage steps: −30 mV to −110 mV in −10 mV steps, 1 s duration). Red traces: responses after application of 300 μM 5-HT to the soma and axon. (**b**) Red, maximum I_h (red) during 5-HT application; gray, instantaneous leak current (**c**) Plot of normalized conductance shows that $V_{1/2}$ of I_h (dotted lines) shifts negatively after 5-HT application (n=6). (**d-f**) Identical protocol and analyses as in **a-c** with 10 μM WAY100135, a 5-HT$_{1A}$ receptor antagonist (brown traces and symbols, n=6). Neither the maximum current nor activation range of I_h is altered in the presence of WAY100135. (**g,h**) Group data averaged 11-13 minutes after 5-HT application for the experiments shown in **a-f** (5-HT: ΔMax. I_h, $p = 0.02$; ΔInst. Leak, $p = 0.77$; Δ$V_{1/2}$, $p = 1.8E{-}05$; n=6. 5-HT/WAY: ΔMax. I_h, $p = 0.74$, ΔInst. Leak, $p = 0.45$, Δ$V_{1/2}$, $p = 0.07$; n=7). One-way repeated measures ANOVA. Error bars indicate SEM. * $p<0.05$, *** $p<0.001$. (**i**) Group data for fast and slow time constants and relative amplitude in the presence of 5-HT and 5-HT with WAY (τ_{fast}: CTL vs. 5-HT, $p = 0.01$; CTL vs. 5-HT/WAY, $p = 0.0006$; τ_{slow}: CTL vs. 5-HT, $p = 0.003$; CTL vs. 5-HT/WAY, $p = 0.16$; [A_{fast}/(A_{fast}+A_{slow})]: CTL vs. 5-HT, $p = 0.0005$; CTL vs. 5-HT/WAY, $p = 0.21$; n=6). 2-tailed paired *t* test. Error bars indicate SEM. * $p<0.05$, *** $p<0.001$

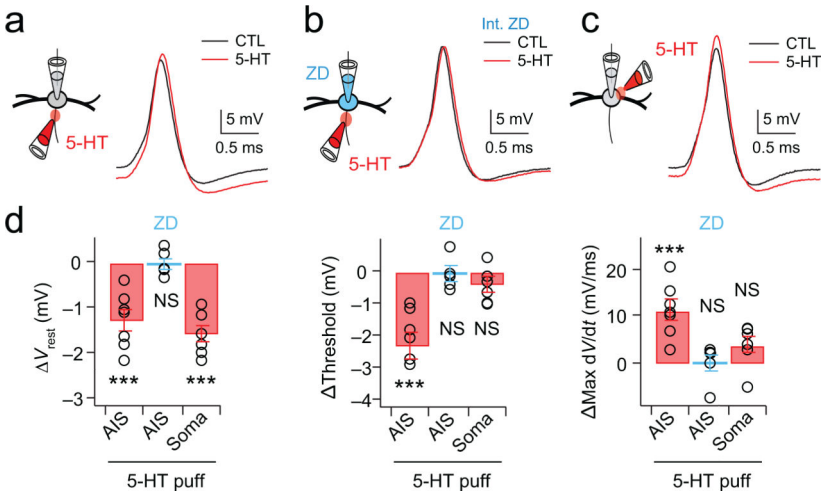

Figure 7. Spike threshold can be controlled by serotonergic modulation of HCN channels in the AIS

(**a**) Focal application of 300 μM 5-HT onto the AIS (red traces) hyperpolarizes the resting membrane potential as well as action potential threshold as compared to the ACSF control (black traces). Vrest = –58 mV and –61 mV for control and 5-HT, respectively. (**b**) The shape and properties of spikes are not altered when 5-HT was applied to the AIS while recording with a pipette solution containing 20 μM ZD7288. Vrest = –59 mV for both control and 5-HT conditions. (**c**) Focal application of 300 μM 5-HT to the soma on the opposite side of the AIS hyperpolarizes the resting potential but does not alter spike threshold or shape. Vrest = –55 mV and –57 mV for control and 5-HT, respectively. (**d**) Group data for focal 5-HT application to the AIS in control ACSF (ΔVrest, $p = 0.001$; ΔThreshold, $p = 0.002$; ΔMax dV/dt, $p = 0.002$; n=7), internal ZD7288 (ΔVrest, $p = 0.82$; ΔThreshold, $p = 0.78$; ΔMax dV/dt, $p = 0.84$; n=5), and somatic application (ΔVrest, $p = 0.01$; ΔThreshold, $p = 0.08$; ΔMax dV/dt, $p = 0.71$; n=6). Error bars indicate SEM. *** $p < 0.001$.

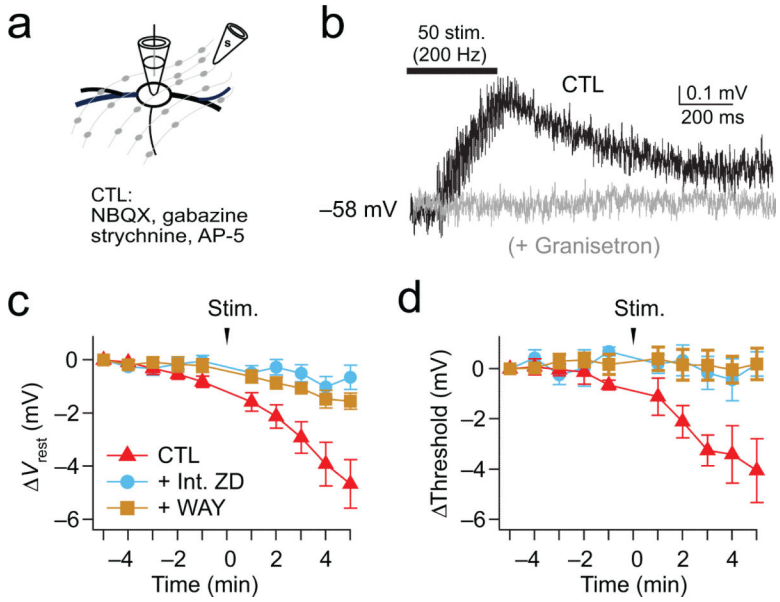

Figure 8. Axonally stimulated release of serotonin modulates the resting potential and spike threshold of MSO neurons

(**a**) Axonal stimulation (200Hz, 50 pulses) of serotonergic fibers. Excitatory and inhibitory inputs are blocked with 10 μM NBQX, 50 μM AP-5, 5 μM gabazine, 1 μM strychnine. (**b**) Response to a train of contralateral synaptic stimuli in ACSF (Black) and 100 μM granisetron (gray), a blocker of ionotropic 5-HT3 receptors. (**c,d**) Resting potential and spike threshold were monitored once per minute before and after 200 Hz electrical stimulation of serotonergic axons (50 stimuli). Action potentials were induced via simulated EPSCs injected through the pipette into the soma. At 5 min. after stimulation, changes in both resting potential and spike threshold typically induced by serotonin release (red) could be blocked by 68% and 95%, respectively, in the presence of 0.1 μM WAY100135 (brown) or 20 μM ZD7288 (blue) dialyzed internally through the pipette (Ctl: $p = 0.002$ and 0.009 for ΔVrest and ΔThreshold, n=7; WAY, $p = 0.0039$ and 0.81 for ΔVrest and ΔThreshold, n=8; Int. ZD: $p = 0.40$ and 0.56 for ΔVrest and ΔThreshold, n=8). 2-tailed paired *t* test. Error bars are SEM.